Journal of Photochemistry & Photobiology, A: Chemistry 404 (2021) 112913

Contents lists available at ScienceDirect

Journal of Photochemistry & Photobiology, A: Chemistry

journal homepage: www.elsevier.com/locate/jphotochem

Coumarin-based quantification of hydroxyl radicals and other reactive species generated on excited nitrogen-doped TiO_2

Abdul Wafi [a,d], Erzsébet Szabó-Bárdos [a], Ottó Horváth [a,*], Éva Makó [b], Miklós Jakab [b], Balázs Zsirka [c]

[a] Department of General and Inorganic Chemistry, Center for Natural Sciences, University of Pannonia, H-8210 Veszprém, POB. 1158, Hungary
[b] Department of Materials Engineering, Research Center for Engineering Sciences, University of Pannonia, H-8210 Veszprém, POB. 1158, Hungary
[c] Laboratory for Surfaces and Nanostructures, Research Center for Biochemical, Environmental and Chemical Engineering, University of Pannonia, H-8210, Veszprém, POB. 1158, Hungary
[d] Laboratory of Pharmaceutical Chemistry, Department of Pharmacy, Universitas Islam Negeri Maulana Malik Ibrahim Malang, 65144, Malang, Indonesia

ARTICLE INFO

Keywords:
Coumarin
OH radical formation
Visible-light photoactivity
Nitrogen-doped TiO_2
Synthesis conditions

ABSTRACT

In order to extend the photoactivity of titanium dioxide into the visible region, highly porous nitrogen-doped TiO_2 catalysts ($NTiO_2$) were successfully synthesized by a modified co-precipitation method with ammonium hydroxide as a nitrogen source. Different approaches such as dosing order of the reagents and temperature of the synthesis, calcination period and temperature were tested to examine the optimum outcome regarding photocatalytic OH radical formation under UV and visible light. Coumarin as a traditional probe for this purpose was applied; measuring the luminescence of 7-hydroxycoumarin produced in the reaction with OH radicals, beside the formation of other hydroxylated derivatives. Only a few percentages of the coumarin molecules reacted with OH radicals, while most of them underwent reactions with other photogenerated species such as electrons (anaerobic/aerobic) and superoxide anion radicals (aerobic). Accordingly, our observations suggest that coumarin can also be used as a probe to quantify the formation of other reactive species. The results were obtained from the difference between the amounts of degraded coumarin and hydroxylated coumarin derivatives formed during photocatalytic experiments. These coumarin-based quantifications of photoactivity was applied for the characterization of the prepared nitrogen-doped TiO_2 catalysts ($NTiO_2$). In addition, material analysis (X-ray diffraction, scanning electron microscopy, energy dispersive X-ray spectrometry, and Fourier transform infrared spectroscopy) showed that crystallinity and nitrogen content were found to be crucial features in the photocatalytic performance of the catalysts.

1. Introduction

Surface waters are polluted with considerable amounts of toxic or dangerous materials (mostly of industrial origins), which cannot be appropriately removed by conventional cleaning technologies. Hence, increasing demands have arisen to develop new procedures, which are environmentally friendly, using little or no chemical additives, economical and efficient against a wide range of organic compounds. Possible techniques may be membrane technology, vacuum evaporation, biological treatment and photocatalysis. Photocatalytic methods have been proved to be suitable for the treatment of water polluted with inorganic and organic contaminants, such as various dyes, pharmaceuticals and pesticides [1,2]. In heterogeneous photocatalytic methods applied for the degradation of various organic pollutants, the most frequently utilized catalyst is titanium dioxide, TiO_2.

TiO_2 is widely used as a photoactive semiconductor, mostly in suspension form. Irradiation in the near UV range generates electron-hole pairs in the TiO_2 nanoparticles. These opposite charges may recombine or, reaching the surface of the catalyst particle, can participate in redox reactions with H_2O, OH^- or dissolved O_2, producing highly reactive species such as hydroxyl radical ($^{\bullet}OH$ or OH radical) and superoxide radical anion ($^{\bullet}O_2^-$), which efficiently oxidize organic

* Corresponding author at: Department of General and Inorganic Chemistry, Center for Natural Sciences, University of Pannonia, P. O. Box 1158, H-8210, Veszprém, Hungary
E-mail addresses: wafi@farmasi.uin-malang.ac.id (A. Wafi), bardose@almos.uni-pannon.hu (E. Szabó-Bárdos), horvath.otto@mk.uni-pannon.hu (O. Horváth), makoe@almos.uni-pannon.hu (É. Makó), jakab.miklos@mk.uni-pannon.hu (M. Jakab), zsirkab@almos.uni-pannon.hu (B. Zsirka).

https://doi.org/10.1016/j.jphotochem.2020.112913
Received 10 July 2020; Received in revised form 8 September 2020; Accepted 10 September 2020
Available online 23 September 2020

pollutants. In addition, contaminants adsorbed on the surface of the catalyst may also react directly with the photochemically produced holes and electrons, promoting the processes of mineralization [3].

However, one of the drawbacks of pure TiO_2 is that it can only be activated by UV illumination, due to its high band-gap energy (3.0 eV for rutile phase and 3.2 eV for anatase phase). This problem leads to a considerable increase in the operation costs [4].

Several TiO_2 modifications have been carried out in order to narrow the band-gap energy; doping with both metal and nonmetal elements is a very promising approach to increase the spectral performance of TiO_2 by shifting its light absorption to the visible region [5]. Numerous nonmetal elements, including N, F, S, C, and P, have been explored, which proved to be appropriate dopants being able to extend the light absorption edge of TiO_2 to the region of visible light, hence, to improve the activity of this photocatalyst. It has been reported that non-metal dopants induce visible-light absorption by either introducing localized electronic states within the band gap or promoting electrons to the conduction band. Nitrogen has been intensively used as a dopant for the modification of titanium dioxide materials, due to its atomic size comparable with that of oxygen, high electronegativity and ionization energy, marked thermal stability and cost-effectiveness [6,7].

Various methods have been applied for preparation of nitrogen-doped TiO_2 ($NTiO_2$), including sol-gel [8–11], hydrothermal [12,13], co-precipitation [14,15] as well as vapor deposition and calcination of $Ti(OH)_4$ under nitrogen atmosphere [7]. Among these synthesis methods, co-precipitation is an easy and convenient approach to prepare $NTiO_2$.

Several organic model compounds have been used to study the photocatalytic performances of $NTiO_2$ catalysts such as Rhodamine B (RhB) [14,16], Methylene blue (MB) [8,17], Methyl orange [18] and Eriochrome black-T [19]. However, those dye compounds can only be used for such a purpose with care because the process involves competing light absorptions by the dyes and the catalyst. Dyes absorb a significant fraction of the light used to excite the catalyst. Hence, the initial concentration of the dyes must be kept at low. Additionally, the dyes may function as sensitizers in the visible range, which, however, can increase the photocatalytic activity. Therefore, to avoid both inner filter effect and possible sensitization, other organic model compounds such as chemical probes must be applied that do not absorb at the irradiation wavelengths.

A number of chemical probes have been used to quantify the photocatalytic efficiency as well as to identify the reactive oxygen species (ROS). Coumarin has been used as an adequate probe to assess the photocatalytic formation of OH radicals, which play an important role in the photocatalytic oxidation. Several hydroxylated coumarins (OHC) are formed in the reaction between coumarin and OH radical as shown in Fig. S1 in the Supplementary Information (SI) [20,21]. One of the products, 7-hydroxycoumarin (7-OHC), produces intensive emission, which can be recorded by using spectrofluorometer. However, most of the previous works mainly focused only on the identification of OH radicals, which converted coumarin to 7-OHC with less than 2% efficiency [13,20–22]. Hence, it is essential to study the photocatalytic pathways and the efficiencies of the reactions of coumarin with both OH radicals and other reactive species generated in TiO_2 based photocatalytic systems.

In this work, visible- and UV-light active, highly porous $NTiO_2$ microparticles were synthesized by co-precipitation method, using titanium (IV) isopropoxide as an economical precursor and ammonium hydroxide as a nitrogen source. The optimization parameters such as dosing order, synthesis temperature, and calcination period were evaluated regarding the photocatalytic formation of OH radicals in the coumarin solution. Furthermore, the effects of calcination temperature on the morphological, structural, optical, and photocatalytic properties of the prepared $NTiO_2$ catalysts were investigated and discussed in details.

In addition, the reactions of coumarin with both OH radicals and other photogenerated reactive species were studied. The emission of 7-OHC (produced by OH radicals) and the change of coumarin concentration during the irradiation were recorded in order to study the photocatalytic pathways. The difference between the concentrations of the coumarin degraded and the OH radicals formed was evaluated to determine the formation of other reactive species such as photogenerated electrons (anaerobic/aerobic) and superoxide anion radicals (aerobic).

2. Materials and Methods

2.1. Materials

Titanium (IV) isopropoxide ($Ti[OCH(CH_3)_2]_4$) 98 % was purchased from Acros Organic (China) and used as titanium precursor. Ammonium hydroxide (NH_4OH) 25% was used as nitrogen source (pure reagent grade) and obtained from Scharlab Hungary Ltd. Nitric acid (HNO_3) 65% was supplied by VWR International. Coumarin ($C_9H_6O_2$) was purchased from Carlo Erba Reagents (France). The 7-hydroxycoumarin ($C_9H_6O_3$) 99% was obtained from Sigma-Aldrich. Barium sulphate ($BaSO_4$) used in this study was purchased from Reanal (Hungary). High-purity water used in these experiments was double distilled and then purified with a Milli-Q system. Compressed air or argon was bubbled into the reaction mixtures from gas bottles.

2.2. Preparation of $NTiO_2$

The preparation of $NTiO_2$ was realized by using a previous method [14] with numerous modifications. The preliminary experiment was conducted in the different synthesis temperature and dosing order step and calcination period.

Synthesis temperature was adjusted to 0, 10 and 25 °C during preliminary experiment. In the first dosing order, 2 mL of titanium (IV) isopropoxide (TTIP) was incorporated into 50 mL of distilled water under continuous stirring for 10 min. Subsequently, 20 mL of nitric acid (65 %) was added to the white suspension, which, thus, turned into a transparent solution. Afterward, ammonium hydroxide 25 % (85 mL) was slowly added to the solution and magnetically stirred for 60 min [14]. In the second dosing, the order of the synthesis steps was modified by starting from nitric acid, ammonium hydroxide, distilled water, and TTIP.

Furthermore, the precipitate obtained from final mixture was vacuum filtered and dried at 40 °C for 24 h. Then the dried $NTiO_2$ was calcined at 150, 250, 350, 400, 450, 500 and 650 °C for different periods of 30, 60, 120 and 240 min in air atmosphere with a heating rate of 2 °C min^{-1} (in a Nabertherm P330 furnace, Germany). The $NTiO_2$ catalysts obtained at different calcination temperatures are shown in Fig. S2. For comparison, undoped TiO_2 was also prepared in a similar way by addition of distilled water instead of ammonium hydroxide and nitric acid.

2.3. Reactor and photocatalytic experiments

Photochemical experiments were carried out by using a laboratory-scale reactor with a volume of 50 mL, (Fig. S3) and in all experiments air or argon (Ar) was continuously bubbled into the reaction mixture. The flow rate of gas was 20 $L.h^{-1}$.

Visible ($\lambda_{max} = 453$ nm; 3 × 7 W) or UV ($\lambda_{max} = 390$ nm; 60 W) LEDs were used as light sources (Fig. S4). The lamp was located at a distance of ~10 cm from the reactor. The temperature of the reaction mixture was relatively stable during the illumination, only increasing by only 2-3 °C. It has not affected the rate of photochemical and thermochemical reactions.

Initially, 50 mg of catalyst – the concentration of the catalyst was 1 g. L^{-1} in all experiments – was placed in 10 mL distilled water and mixed under sonication for 30 min, followed by stirring overnight to homogenize the particles. OH radicals might be formed during sonication,

however, they would recombine in the absence of scavenger. Afterwards, 40 mL of the organic model compound – the initial concentration of coumarin was 0.8×10^{-4} mol.L^{-1} – was added to the suspension and left in the dark for 30 min to establish an adsorption-desorption equilibrium at room temperature.

Before and during the irradiation, 3 mL of samples were taken through a septum with a syringe and filtered by a Millipore Millex-LCR PTFE 0.45 μm membrane filter.

2.4. Analytical procedures

In this work, coumarin was used to react directly with OH radicals generated during the irradiation of the photocatalysts, producing strongly emissive 7-hydroxycoumarin (7-OHC) [21]. The emission of 7-OHC (excited at 332 nm) was determined by spectrofluorometer (PerkinElmer LS50B).

Then the absorbances of the residual coumarin were measured by using a UV-Vis spectrophotometer (Scinco S-3100). The molar absorption coefficient (ε) of the 7-OHC compound at 277 nm was significantly lower (3209 L.mol^{-1}. cm^{-1}) than that of the coumarin compound (11308 L.mol^{-1}. cm^{-1}), therefore at low concentrations ($c = 10^{-5}$ mol.L^{-1}) the resulting 7-OHC did not significantly alter the light absorption. No spectrum distortion appeared at the maximum absorption of the 7-OHC ($\lambda = 324$ nm, ε(coumarin) = 5122 L.mol^{-1}. cm^{-1}; ε(7-OHC) = 11405 L. mol^{-1}. cm^{-1}) (Fig. S5). The concentration of the generated 7-OHC and the residual coumarin were calculated by using calibration curves (Fig. S6). These were determined by plotting the emission intensity values at 453 nm as a function of the concentration of 7-OHC and the absorbance at 277 nm as a function of the coumarin concentration.

The degradation efficiency of the coumarin (D(t), %) was calculated by using Eq. 1.

$$D(t)\ (\%) = \frac{C_0 - C_t}{C_0} \quad (1)$$

where C_0 and C_t are the initial and actual concentrations of the starting compound, respectively [23].

2.5. Characterization

The analyses of morphology and elemental composition of the catalysts were carried out by using scanning electron microscopy coupled with energy-dispersive x-ray spectroscopy (SEM/EDX). An Apreo SEM (ThermoFisher Apreo S scanning electron microscope) equipped with Octane Elect Plus EDX (AMETEK) was used at 5.0 kV for imaging and 25.0 kV for elemental analysis. For thermogravimetric analysis (TG) and differential thermal analyses (DTA), a Derivatograph-C type thermoanalytical instrument (Hungarian Optical Works) was applied in the temperature range of 20–1000 °C, with 5 °C min^{-1} heating rate and dynamic synthetic air atmosphere, using open ceramic crucibles. The Fourier transform infrared spectroscopy measurements with attenuated total reflection (FTIR-ATR) were carried out by using a BRUKER Vertex 70 type spectrometer with a single reflection Bruker Platinum diamond ATR adapter. The spectra of the ground samples were recorded at a resolution of 2 cm^{-1}, with a room temperature DTGS detector by averaging 512 scans. The crystal structure of $NTiO_2$ catalysts were examined by using XRD (Philips PW 3710 type powder diffractometer) with a Cu-Kα radiation source ($\lambda = 1.5405$ Å). Diffraction peaks were recorded from 10° to 70° and used to determine the structure of catalysts. The crystallite size values were calculated using the Scherrer equation (Eq. 2):

$$D = \frac{0.94\lambda}{\beta\cos(\theta)} \quad (2)$$

where D is the crystal size, λ is wavelength of the X-ray source (Cu-Kα = 1.5405 Å), β is the full width half-maximum (FWHM) of the diffraction peak and θ is the diffraction angle [24].

Diffuse reflectance spectra (DRS) were recorded on a luminescence spectrometer (PerkinElmer, USA) equipped with an integrating sphere. The band-gap energy was calculated using Tauc plot of square of the Kubelka-Munk function against photon energy [25]. The details of the calculation are described in Text S1 of the SI.

3. Results and Discussion

3.1. Preliminary study

3.1.1. Morphology

In this work, $NTiO_2$ catalyts were synthesized via different dosing orders including TTIP-H_2O-HNO_3-NH_4OH (first dosing order) and HNO_3-NH_4OH-H_2O-TTIP (second dosing order). SEM measurements exhibited that all samples (prepared by both first and second dosing orders) mainly contained amorphous microparticles with various sizes within ~ 2-100 μm. The particle sizes are similar to those previously reported by Gurkan et al. [26], in the case of which wet impregnation method was applied. The $NTiO_2$ catalyst consisted of spherical particles with sizes up to 50-100 μm. Microsheets and nanorice grains were obtained for the morphology of the $NTiO_2$ catalyst prepared by hydrothermal method with average lengths of 3.5 μm and 250 nm, respectively [12,13].

Noticeably, the dosing order during the synthesis in the preliminary experiments significantly affected the surface morphology. A non-porous material was obtained by the first dosing order (TTIP-H_2O-HNO_3-NH_4OH) as displayed in Fig. 1a. However, $NTiO_2$ catalysts prepared by the second dosing order (HNO_3-NH_4OH-H_2O-TTIP), displayed a highly porous surface after and before calcination at 450 °C as shown in Figs. 1b-c. Interestingly, porous structures were also observed in the undoped TiO_2 (450 °C), and the pore sizes were similar to those of the $NTiO_2$ catalyst (Fig. 1d). Hence, it can be concluded that the formation of pores was not influenced by the nitrogen doping. The pores might be formed during the exothermic reaction between the titanium precursor and water.

The average pore sizes of undoped TiO_2 were stable during the calcination processes, but it increased for the $NTiO_2$ catalysts. The average pore diameters of $NTiO_2$ before and after calcination were about 1 and 3 μm, respectively. Thermal analysis revealed a weight loss of $NTiO_2$ catalysts at 302-464 °C, which can be attributed to the removal of ammonia (from nitrogen precursor) as shown in Text S2 and Fig. S7 [27]. It is also reported that the calcination process increased the average pore sizes [14,28,29].

3.1.2. Photocatalytic activity

The photocatalytic activity of catalysts were assessed by measuring the OH radicals under visible and UV light. OH radical formation is usually considered as a key process characterizing the photocatalytic activity [13]. It is well known that OH radical is one of the highly ROS in the photocatalysis that attacks the organic model compounds, resulting in the degradation of contaminants [38,39]. Coumarin was used as the scavenger of OH radicals and the concentrations of 7-OHC were calculated from the emission data at 453 nm by using a calibration curve (Fig. S6), and the initial rates (v_0) were determined from the slope of linear regression equation. The concentration of 7-OHC was found to be proportional to the amount of OH radical produced.

Preliminary experiments were carried out to find the optimum of dosing order, synthesis temperature (Text S3) and calcination period (Text S4) of $NTiO_2$ (calcined at 450 °C) from the viewpoint of photoactivity. The $NTiO_2$ catalyst prepared by using the second dosing order (HNO_3-NH_4OH-H_2O-TTIP) exhibited a higher photoactivity under visible light, which might be attributed to the surface morphology. The porous surface properties are important in the photocatalytic performances because the large surface area can improve the adsorption of pollutants compared to the case of non-porous materials. The surface

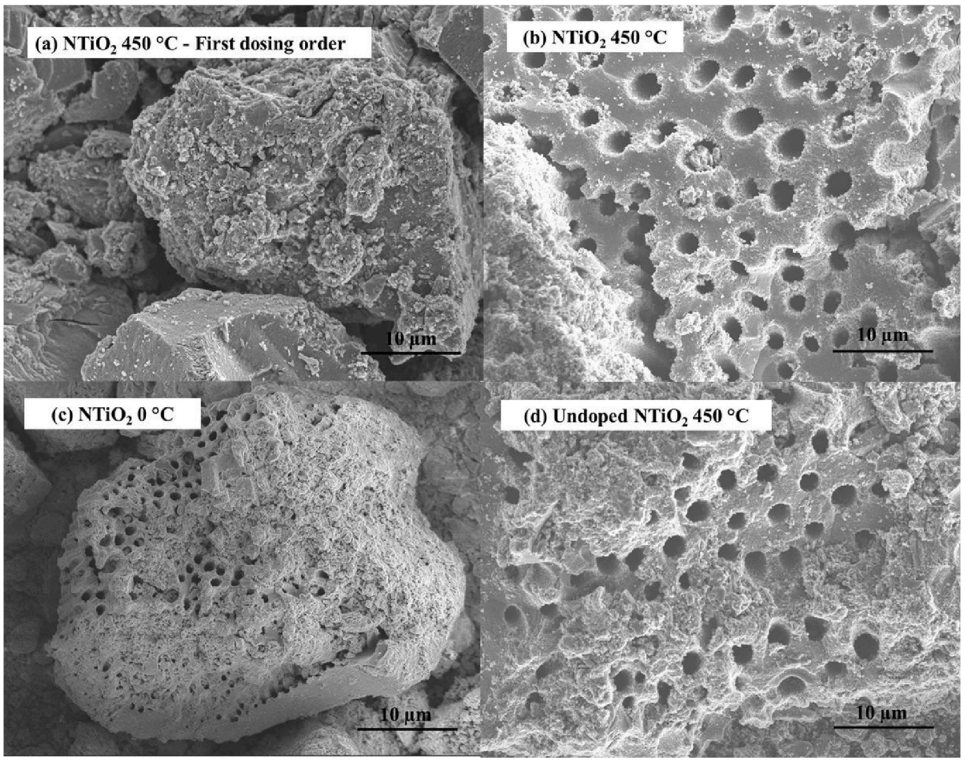

Fig. 1. SEM morphology of catalysts prepared by (a) first and (b-d) second dosing order.

area can strongly be related to the active sites which are crucial in trapping photoinduced carriers and prolonging their lifetime [30]. Liu et al. reported that the mesoporous nitrogen-doped TiO_2 has a superior photocatalytic activity under both UV and visible irradiation, compared to the undoped TiO_2 [31].

In addition, the synthesis temperature of 10 °C and 30-min calcination period were found to be an optimum for 7-OHC formation under visible light as shown in Figs. S8-S9.

3.2. Effect of calcination temperature

3.2.1. Material properties

The optimum parameters determined in the preliminary experiments were used for further investigations regarding the effect of the calcination temperature on the material properties and photoactivity under both visible and UV light.

Firstly, the changes of the vibrational states in the $NTiO_2$ catalyst were measured by using FTIR spectroscopy. Fig. 2a exhibits the FTIR spectra of undoped TiO_2 and $NTiO_2$ calcined at different temperatures.

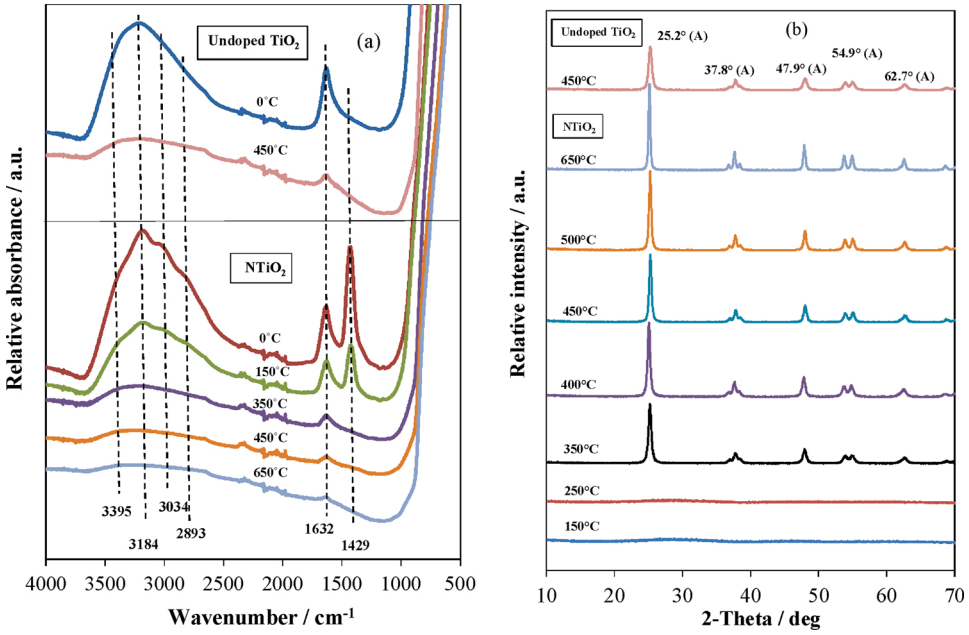

Fig. 2. (a) FTIR and (b) XRD spectra of undoped TiO_2 and $NTiO_2$ calcined at various temperatures.

For the undoped TiO_2 calcined at 0 °C (i.e., non-calcined), there are two characteristic peaks; a relatively sharp one at 1632 cm^{-1} and a broad one between 3000 to 3500 cm^{-1}, which correspond to O-H bending and OH stretching vibrations, respectively. For the $NTiO_2$ catalyst, an additional peak appeared at 1429 cm^{-1} (N-H bending) and the broad band resolved into four ones at 2983, 3034, 3184, 3395 cm^{-1} which can be assigned to N-H stretching overlapped with OH vibrations. The intensity of these peaks decreased at higher calcination temperatures and started to disappear up to 350 °C. It might be due to the transformations of NH groups, resulting in new bonds of nitrogen (e.g., Ti-N/N-Ti-O), the vibrations of which were not detectable at the measurement parameters applied [10,14].

The structural properties of the catalysts were determined by using XRD measurements. Fig. 2b illustrates the XRD patterns of the $NTiO_2$ catalysts calcined at various temperatures. Pure anatase phase was obtained for all catalysts except for the ones calcined at 150 °C and 250 °C, which were of amorphous titania. The diffraction peaks located at 25.2°, 37.8°, 47.9°, 54.9° and 62.7° are mainly related to the anatase phase (JCPDS card no. 21-1272) with Miller indices labeled as (101), (004), (200), (211) and (204), respectively. There was not any phase transformation of the catalysts from anatase to rutile or brookite during calcination up to 650 °C. Generally, the phase transformation of pure TiO_2 from anatase to rutile occurs between 500 °C to 600 °C, and completely transforms to rutile at 600 °C [32,33]. From our results, it clearly indicates that the nitrogen doping in TiO_2 inhibited the phase transformation from anatase to rutile, in accordance with a quite recent observation [13].

The peak intensity of anatase (101) increases and the width of (101) plane becomes narrower with increasing calcination temperature. This tendency can be attributed to the growth of the average diameter of the crystaline particles upon temperature rising. The crystallite sizes increased from 15 nm (350 °C) to 27.5 nm (650 °C) as summarized in Table 1. In comparison, according to a previous work, the crystallite size of the standard Degussa P25 TiO_2 was approximately 79.7 nm [34].

Energy dispersive X-ray spectrometry (EDX) was applied to investigate the elementary composition of $NTiO_2$ calcined at various temperatures. The percentage of nitrogen content significantly dropped from 14.09 to 5.50 wt% upon increasing the calcination temperature from non-calcined to 450 °C (Table 1). In addition, a nearly constant nitrogen content (around 3.45 ± 0.16 wt%) was obtained above a calcination temperature of 500 °C. It exhibited that not only water molecules were released from $NTiO_2$ during the heating process, but also the nitrogen content changed. The loss of nitrogen could be replaced by oxygen from air upon increasing calcination temperature [35].

The band-gap energies were determined by the analysis of diffuse reflectance spectra, applying the Kubelka-Munk function (Fig. S8). Generally, nitrogen doping slightly reduced the band-gap energy of TiO_2 into 3.01-3.18 eV. This phenomenon is in accordance with previous observations, according to which the obtained band-gap energy of $NTiO_2$ catalysts were 2.94-3.18 eV [8,13,14,36]. Those catalysts exhibited excellent photocatalytic performances in the degradation of MB, RhB, and ciprofloxacin, under both visible and UV light.

Upon enhancing the calcination temperature, the band-gap energy indicates a moderate, but monotonous increase (Table 1). It is strongly related to the decrease of the nitrogen content. It is well known that nitrogen as doping element induces the formation of a new energy level (localized N2P state) in the valence band, extending the light absorption into the visible range [35,37]. These results can also be used to verify that the higher calcination temperature could potentially increase the band-gap energy, due to the nitrogen loss.

Table 1
Summary of characteristic data for $NTiO_2$ and TiO_2.

Calcination temperature / °C	Band-gap Energy / eV	Crystalline phase	Crystallite size / nm	Nitrogen content / wt%
non-calcined	-	amorphous	-	14.09
150	3.01	amorphous	-	9.53
250	3.03	amorphous	-	8.88
350	3.05	pure anatase	15.06	8.41
400	3.11	pure anatase	17.22	7.20
450	3.12	pure anatase	19.20	5.50
500	3.13	pure anatase	20.70	3.30
650	3.17	pure anatase	27.53	3.61
450*	3.18	pure anatase	13.93	0.00

* Undoped TiO_2 calcined at 450 °C

3.2.2. Photocatalytic activity

The photocatalytic activity of these $NTiO_2$ catalysts prepared in the various calcination temperatures were evaluated under both visible and UV light (Fig. S11). Its effect on the initial rate (v_0) of 7-OHC formation is shown in Fig. 3. The $NTiO_2$ catalysts calcined at 150 and 250 °C were inefficient regarding the photoinduced OH radical formation, independently of the irradiation wavelength. In addition, the 7-OHC formation gradually rose in the 350-450 °C range and dramatically decreased at 500 to 650 °C under visible-light (Fig. 3a). In contrast, upon UV irradiation, the 7-OHC formation indicated a monotonous and significant increase upon rising the calcination temperature (Fig. 3b). Beside the deviating tendencies, compared to the rates observed under visible light, UV irradiation strongly (more than one order of magnitude) improved v_0 of 7-OHC formation over the $NTiO_2$ catalysts (Table 2). This phenomenon can be attributed to the higher energy of UV compared to that of visible light [40] and to the structural deviations originated from the different nitrogen contents.

Moreover, crystalline phase, cystallite size, nitrogen content, and surface morphology are important features affecting the photocatalytic performances of $NTiO_2$ catalysts. According to the XRD results, all catalysts were transformed into pure anatase phase during calcination at 350 to 650 °C, but they are characterized by different nitrogen contents and crystallinities (Table 1). The crystallite size increased with the rising calcination temperature. The higher crystallite size had a better adsorption, thus inducing a higher photoactivity [41]. Under visible light, the photoactivity increased from 350 °C to 450 °C and significantly decreased from 500 to 650 °C (Fig. 3a). It might be attributed to the decrease of the nitrogen content (Table 1) during calcination, which led to a higher band-gap energy and less light absorption in the visible range [14,35,36,42]. From this point of view, both crystallite size and nitrogen content of the $NTiO_2$ catalysts play crucial roles in the v_0 of OH radical formation (Fig. 4a).

The initial rate of 7-OHC formation under UV light significantly improved by higher calcination temperature. The increase of photoactivity was in line with the increasing of crystallite size under UV light (Fig. 4b). It should also be noted that an increase of the calcination temperature reduces the nitrogen content, which results in only a slight change in the oxidation capacity of the valence band. Nevertheless, it is a general phenomenon that relatively small decreases of the band-gap considerably diminishes the photoactivity in the UV range.

3.3. Photocatalytic pathways

3.3.1. Photocatalytic reactions with coumarin under UV light

One of our main goals was to study the reactions of coumarin as a probe of the photocatalytic activity of the nitrogen-doped titanium dioxide upon both UV- and visible-light irradiations. $NTiO_2$ calcined at 450 °C was applied for these measurements because it displayed the highest photoactivity under visible light. The reaction mixtures were saturated with Ar or air during the irradiations, ensuring anaerobic or aerobic conditions, respectively.

The first measurements were carried out under UV irradiation. The total concentration of the hydroxylated coumarins (OHC) was estimated from the concentration of 7-OHC, the fraction of which was about 29% of all OHC products [20]. Besides, the amount of OH radicals formed

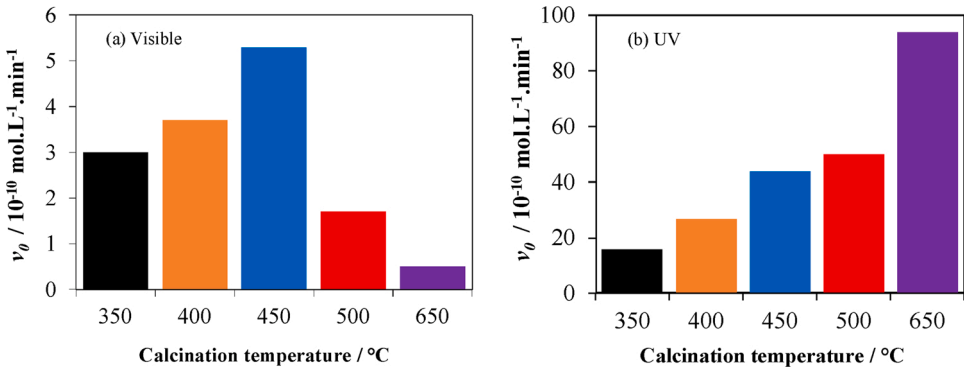

Fig. 3. Effect of the calcination temperature on the initial rate of 7-OHC formation under (a) visible and (b) UV light.

Table 2
Summary of initial rate of 7-OHC formation.

Catalyst	v_0 of 7-OHC formation / 10^{-10} mol.L^{-1}. min^{-1}		Ratio (b:a)
	(a) Visible	(b) UV	
DP25 TiO_2*	0.2	331.5	1657.5
Undoped TiO_2 450 °C*	0.4	51.1	127.8
$NTiO_2$ 350 °C	3.0	15.7	5.2
$NTiO_2$ 400 °C	3.7	26.5	7.2
$NTiO_2$ 450 °C	5.3	43.7	8.3
$NTiO_2$ 500 °C	1.7	49.9	29.4
$NTiO_2$ 650 °C	0.5	93.8	187.6

* Data can be found in Fig. S7.

was obtained from the total OHC concentration. The efficiency of OH radical trapping by coumarin to produce OHC was found to be 6.42% of all OH radical formation [43]. In addition, under anaerobic conditions, 1 molecule of OHC is obtained from the reaction between 2 molecules of OH radicals and 2 molecules of coumarin. However, 2 molecules of OH radicals and 1 molecule of coumarin are required to produce 1 molecule of OHC in aerobic atmosphere [20]. Considering these facts, the concentration of OH radicals formed in the latter system could be calculated by using Eqs. 3–4:

$$[\mathrm{OHC}] = \frac{100}{29} \mathrm{x} \left[7 - \mathrm{OHC}\right] \quad (3)$$

$$\left[^{\bullet}\mathrm{OH}\right] = \frac{2\ \mathrm{mol}}{1\ \mathrm{mol}} \mathrm{x} \frac{100}{6.42} \left[\mathrm{OHC}\right] \quad (4)$$

As shown in Fig. 5a, the 7-OHC formation in the absence of O_2 exhibits a gradual increase during the UV irradiation. After 60-min irradiation, the concentration of 7-OHC formation reached 1.30×10^{-7} mol.L^{-1} and those for OHC and OH radical were 4.48×10^{-7} mol.L^{-1} and 139.82×10^{-7} mol.L^{-1}, respectively. The initial rate of OH radical formation was 2.24×10^{-7} mol.L^{-1}. min^{-1}.

Generally, in the presence of O_2 the concentration of 7-OHC or OH radical increased in the first period of irradiation time as shown in Fig. 5b. The concentration of 7-OH reached to 2.66×10^{-7} mol.L^{-1} after 60-min irradiation, and for OHC and OH radical were 9.18×10^{-7} mol.L^{-1} and 286.20×10^{-7} mol.L^{-1}, respectively. The enhancement of the photoactivity might be attributed to better charger separation of photogenerated electron-hole pairs leading to higher OH radical formation. The initial rate (v_0) of OH radical formation was 4.69×10^{-7} mol.L^{-1}. min^{-1}. Furthermore, after the first period, a declining phase was observed due to the low rate of 7-OHC formation. The decrease of 7-OHC concentration can be attributed to the relative excess of ROS (OH radical, superoxide anion radical or H_2O_2) which can further degrade 7-OHC itself or attack the intermediates of reactions and convert those into various products other than 7-OHC [44,45].

The concentration of coumarin was also measured during the photocatalytic reaction to evaluate the degradation efficiency. As illustrated in Fig. 6a, in anaerobic atmosphere, the total coumarin degradation efficiency after 240-min irradiation and the initial degradation rate (v_0) were 20.2 % and 1.1×10^{-7} mol.L^{-1}. min^{-1}, respectively. However, in aerobic atmosphere, the degradation efficiency of coumarin significantly increased; to 58.6% after 240-min irradiation, with an initial degradation rate of $v_0 = 3.6 \times 10^{-7}$ mol.L^{-1}. min^{-1} (Fig. 6b).

In order to study the photocatalytic degradation pathways of coumarin, all types of OHC formation and coumarin degradation were evaluated. Total coumarin degradation was obtained from the difference between the initial and the actual coumarin concentrations. OHC concentration indicates the amount of coumarin degraded through the

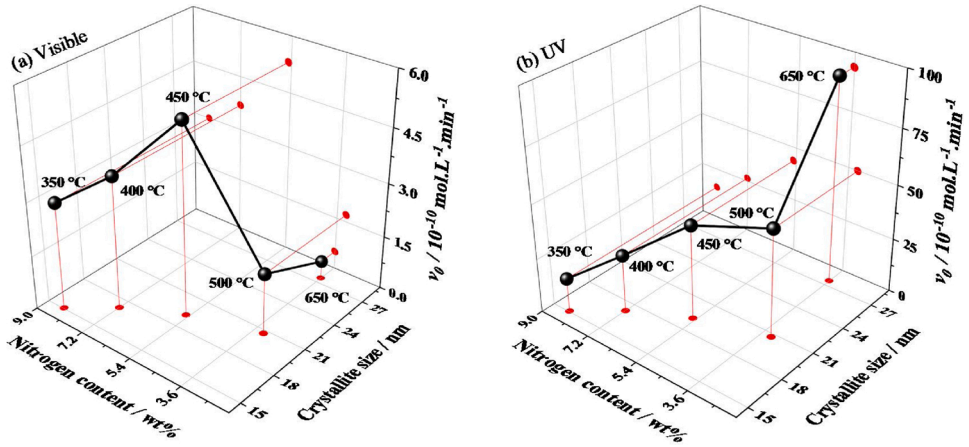

Fig. 4. Correlation of calcination temperature, nitrogen content and crystallite size on the v_0 of 7-OHC formation under (a) visible and (b) UV light.

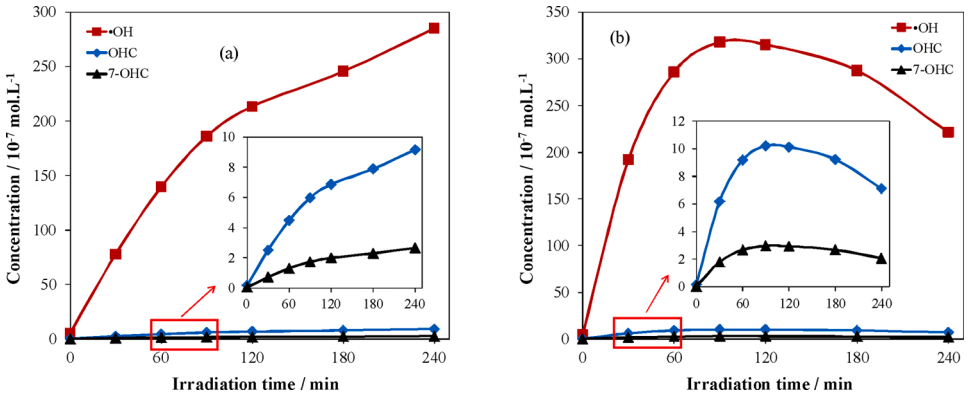

Fig. 5. The concentrations of OH radical, OHC and 7-OHC during UV irradiation of $NTiO_2$ catalyst (calcined at 450 °C) under (a) anaerobic and (b) aerobic conditions. Insets show the plots for OHC and 7-OHC at higher resolution.

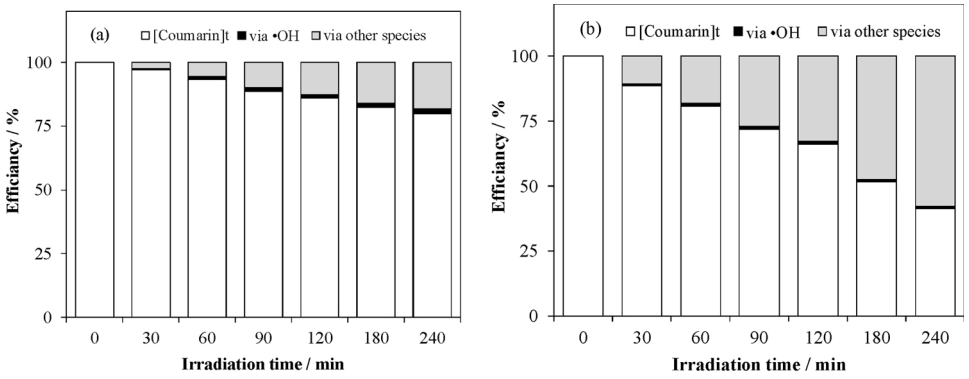

Fig. 6. Efficiency of coumarin degradation during UV irradiation of $NTiO_2$ catalyst (calcined at 450 °C) under (a) anaerobic and (b) aerobic conditions. (Total coumarin degradation = black + gray).

reactions with OH radicals. The difference between the total coumarin degradation and the OHC concentration suggested the coumarin degradation through the reaction with other reactive species (Fig. 6). Under anaerobic condition, total coumarin degradation was about 6.65% after 60 min irradiation, while the coumarin degradation in reactions with OH radicals and other reactive species were 0.97% and 5.67%, respectively. A similar phenomenon was also observed in aerobic atmosphere, where only about 1.01% of coumarin reacted with OH radical. Meanwhile, the degradation of coumarin in reactions with other reactive species was 18.24% from the total coumarin degradation of 19.25%. The coumarin degradation via different pathways is summarized in Table 3. The results show that coumarin prefers to react with species other than OH radicals. Zerjav and co-workers studied coumarin as OH radicals probe over pure anatase TiO_2 nanorods. It was found that less than 2% of coumarin was converted into the photoluminescent 7-OHC [22].

As given in Table 3, the efficiency of coumarin degradation through the reaction with OH radicals hardly depended on the presence of oxygen. However, compared to anaerobic, the efficiency of the reaction with other reactive species significantly increased in aerobic atmosphere. As shown in Fig. 7, the initial rate of coumarin degradation via reactions with other reactive species under anaerobic and aerobic conditions were 1.0×10^{-7} mol.L^{-1}. min^{-1} and 2.7×10^{-7} mol.L^{-1}. min^{-1}, respectively.

Generally, photocatalytic reaction was initiated by irradiation of $NTiO_2$ catalyst, producing photo-generated electrons in the conduction band, along with corresponding positive holes in the valence band. In anaerobic atmosphere (Ar), these photo-generated electrons and holes can quickly recombine in the absence of electron scavenger, leading to a low photoactivity (Eqs. 5–6). However, at the same time, coumarin can act as an electron scavenger ($k = 1.6 \times 10^{10}$ L. $mol^{-1}.s^{-1}$ [46]) in the absence of oxygen, forming non-fluorescent products (Eq. 7), while the holes in the valence band react with adsorbed H_2O molecules, leading to the formation of OH radicals (Eq. 8). Various OHC products are formed in the reaction with coumarin as illustrated in Eq. 9 [20].

$$NTiO_2 + h\nu \rightarrow NTiO_2(h_{VB}^{+} + e_{CB}^{-}) \text{ Excitation} \quad (5)$$

$$NTiO_2(h_{VB}^{+} + e_{CB}^{-}) \rightarrow NTiO_2 \text{ Recombination} \quad (6)$$

Table 3
Coumarin degradation via different pathways over $NTiO_2$ calcined at 450 °C, under UV light after 30 and 60-min irradiation time.

Atmosphere	Irradiation time / min	Total coumarin degradation / %	Coumarin degradation via reaction with (a) •OH	(b) other reactive species	Ratio (b:a)
Anaerobic	30	2.96	0.54	2.42	4.47
Aerobic		11.48	0.68	10.80	15.88
Anaerobic	60	6.65	0.97	5.67	5.83
Aerobic		19.25	1.01	18.24	18.06

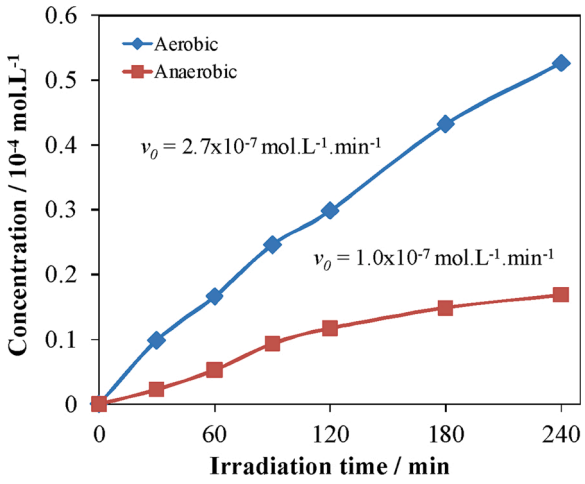

Fig. 7. Irradiation time dependence of concentration of coumarin degraded through the reactions with other reactive species.

$$e_{CB}^- + \text{coumarin} \rightarrow \text{non-fluorescent products} \quad (7)$$

$$h_{VB}^+ + H_2O \rightarrow {}^\bullet OH + H^+ \quad (8)$$

$${}^\bullet OH + \text{coumarin} \rightarrow \text{fluorescent 7-OHC} + \text{other OHC} \quad (9)$$

In case of aerobic atmosphere, oxygen is a powerful electron scavenger, thus extending the lifetime of the photo-generated electron-hole pairs. The rate constant of the reaction between electron and O_2 ($k = 2.3 \times 10^{10}$ L. mol^{-1}.s^{-1} [47]) is higher than that for the reaction of electron with coumarin ($k = 1.6 \times 10^{10}$ L. mol^{-1}.s^{-1} [46]). Taking the concentrations of coumarin and dissolved oxygen (in air-saturated solution at 20 °C), 0.8×10^{-4} mol.L^{-1} and 0.56×10^{-4} mol.L^{-1} respectively, the efficiencies of the reactions of photo-generated electrons with these two species are very similar at the beginning of the irradiation. However, due to the degradation of coumarin, its concentration significantly decreased during the irradiation, hence, more and more photo-generated electrons were converted into superoxide anion radicals (Eq. 10).

$$e_{CB}^- + O_2 \rightarrow {}^\bullet O_2^- \quad (10)$$

Superoxide anion radical can be easily protonated (pKa ($^\bullet HO_2/^\bullet O_2^-$) = 4.8), producing OH radical in the further reaction steps (Eqs. 11–13) [48]. Subsequently, OH radicals formed from hydroperoxyl radical (Eq. 12), the product of protonation of superoxide radical anion (Eq. 11), as well as from the oxidation of H_2O by holes (Eq. 8), easily react with coumarin (Eq. 9) ($k = 2.0 \times 10^9$ L. mol^{-1}.s^{-1} [47]).

$${}^\bullet O_2^- + H^+ \leftrightarrow {}^\bullet HO_2 \quad (11)$$

$${}^\bullet HO_2 + {}^\bullet HO_2 \rightarrow H_2O_2 + O_2 \quad (12)$$

$$H_2O_2 + {}^\bullet O_2^- \rightarrow {}^\bullet OH + OH^- + O_2 \quad (13)$$

However, our results indicated that superoxide anion radicals were predominantly in deprotonated form, owing to the neutral pH (6-7) of the solution during irradiation. Hence, this suggests that the reaction of superoxide anion radicals with coumarin can considerably contribute to its degradation, resulting in non-fluorescent products as shown in Eq. 14 [49,50].

$${}^\bullet O_2^- + \text{coumarin} \rightarrow \text{non-fluorescent products} \quad (14)$$

Therefore, apart from the processes via OH radicals, coumarin degradation in aerobic system is more efficient than in anaerobic one, due to the efficient reaction with superoxide anion radicals. Moreover, dissolved oxygen can significantly increases the oxidative transformation of instable radicals formed in the reactions of coumarin with ROS.

Furthermore, $NTiO_2$ catalysts calcined at various temperatures were also investigated in anaerobic and aerobic atmosphere under UV light (Fig. S12). Regarding the different calcination temperatures, the photoactivity increased upon increasing the calcination temperature in both aerobic and anaerobic systems. $NTiO_2$ calcined at 650 °C showed the best OH radical formation under both anaerobic ($v_0 = 3.08 \times 10^{-7}$ mol.L^{-1}. min^{-1}) and aerobic ($v_0 = 10.08 \times 10^{-7}$ mol.L^{-1}. min^{-1}) conditions as illustrated in Fig. 8a. The degradation of coumarin revealed an identical trend, according to which $NTiO_2$ catalyst calcined at 650 °C exhibited the highest degradation efficiencies after 240 min irradiation; with approximately 26% ($v_0 = 1.3 \times 10^{-7}$ mol.L^{-1}. min^{-1}) in anaerobic atmosphere, while under aerobic conditions the coumarin degradation significantly increased to 93% with the initial degradation rate of $v_0 = 15.1 \times 10^{-7}$ mol.L^{-1}. min^{-1} (Figs. 8b).

The ratio (aerobic/anaerobic) of the OH radical formation was

Table 4
Ratio (aerobic/anaerobic) of OH radical formations over $NTiO_2$ calcined at different temperatures, under UV light.

Calcination temperature / °C	v_0 of OH radical formation / 10^{-7} mol. L^{-1}. min^{-1}		Ratio (b:a)
	(a) Anaerobic	(b) Aerobic	
350	0.84	1.69	2.01
450	2.24	4.69	2.09
650	3.08	10.08	3.27

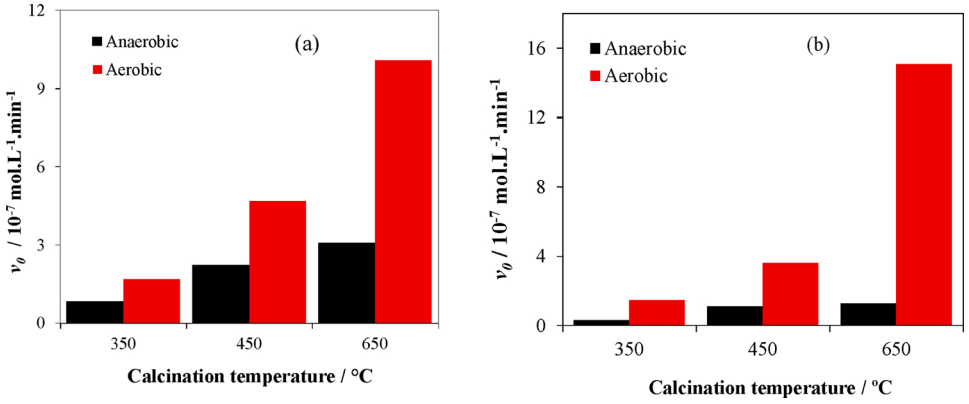

Fig. 8. Initial rates of (a) OH radical formation and (b) coumarin degradation over $NTiO_2$ calcined at different temperatures in aerobic and anaerobic atmospheres, under UV light.

Table 5
Ratio (aerobic/anaerobic) of coumarin degradation over $NTiO_2$ calcined at different temperatures, under UV light.

Calcination temperature / °C	v_0 of coumarin degradation / 10^{-7} mol.L^{-1}. min^{-1}		Ratio (b:a)
	(a) Anaerobic	(b) Aerobic	
350	0.3	1.5	5.0
450	1.1	3.6	3.27
650	1.3	15.1	11.61

determined over $NTiO_2$ catalysts calcined at different temperatures. As given in Table 4, this ratio increased with increasing calcination temperature, where $NTiO_2$ calcined at 650 °C exhibited the highest ratio (3.27).

Similarly, the ratio (aerobic/anaerobic) of coumarin degradation also showed the highest value over $NTiO_2$ calcined at 650 °C as displayed in Table 5. It means that the presence of oxygen (air) could enhance the coumarin degradation over 10 times that of the value in anaerobic system. In addition, the ratio (aerobic/anaerobic) of coumarin degradations was higher than the ratio (aerobic/anaerobic) of OH radical formation. In other words, the production of electrons or superoxide anion radicals was greater than that of OH radicals (7-OHC) over $NTiO_2$ calcined at 650 °C. As shown in Fig. 4b, the nitrogen content drops and the crystallite size increases at high calcination temperature (650 °C). From this point of view, it can be assumed that less nitrogen content and larger crystallite size of $NTiO_2$ are favorable for the generation of more electrons or superoxide anion radicals under UV-light irradiation.

3.3.2. *Photocatalytic reactions with coumarin under visible light*

The OH radical formation was successfully detected by using fluorescence spectrometer in both systems (anaerobic and aerobic). The initial rate of OH radical formation in anaerobic atmosphere was 0.23×10^{-7} mol.L^{-1}. min^{-1} and it increased to 0.7×10^{-7} mol.L^{-1}. min^{-1} upon aeration of the system as shown in Fig. 9. In comparison, the initial rate of OH radical formation in the visible was significantly lower than under UV light. The initial rates of OH radical formation under UV light were 2.24×10^{-7} and 4.69×10^{-7} mol.L^{-1}. min^{-1} for anaerobic and aerobic system, respectively. As a result, the change of coumarin concentration (due to its transformations) could not be reliably detected by using spectrophotometric measurements during the photocatalytic reaction under both anaerobic and aerobic atmosphere.

However, the ratio (aerobic/anaerobic) of OH radical formation under visible light was higher, compared to that in UV light, as

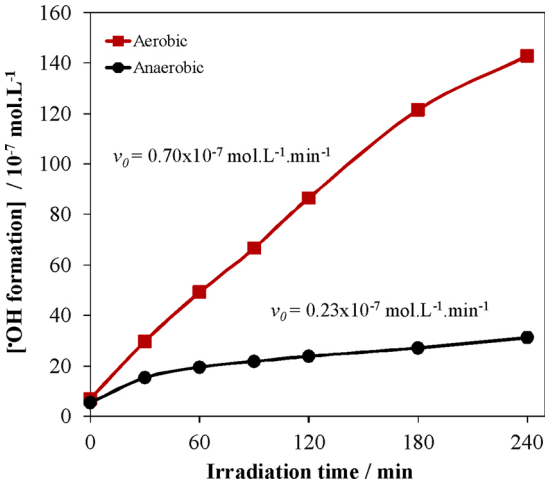

Fig. 9. OH radical formation over $NTiO_2$ (calcined at 450 °C) in aerobic and anaerobic atmosphere under visible light.

Table 6
Formation of OH radicals over $NTiO_2$ (calcined at 450 °C) under visible or UV light in aerobic or anaerobic atmosphere.

Light	v_0 of OH radical formation / 10^{-7} mol.L^{-1}. min^{-1}		Ratio (b:a)
	(a) Anaerobic	(b) Aerobic	
Vis	0.23	0.70	3.04
UV	2.24	4.69	2.09

summarized in Table 6. It shows that in the presence of O_2, the photocatalytic enhancement of OH radical formation over $NTiO_2$ (calcined at 450 °C) under visible light was more favorable than in UV light (3.04 vs. 2.09).

4. Conclusions

Visible- and UV-light-active nitrogen-doped TiO_2 catalysts were successfully prepared by a co-precipitation method, using ammonium hydroxide as nitrogen source. The catalysts displayed high porosity and consisted of pure anatase phases at the calcination temperatures 350-650 °C. The phase transformation from anatase to rutile at high calcination temperature was successfully inhibited due to the presence of nitrogen dopant in TiO_2. The nitrogen content decreased by increasing calcination temperature and strongly related to the photocatalytic efficiency. The $NTiO_2$ catalysts calcined at 450 °C and 650 °C for 30 min showed the highest photocatalytic OH radical formation under visible and UV light, respectively. Coumarin was used for the monitoring of OH radical formation by producing hydroxylated derivatives, but it efficiently reacted with photogenerated electrons and (in aerated system) superoxide anion radicals, too. We have unambiguously proved that coumarin could also be used to estimate the production of other reactive species (i.e. electrons or superoxide anion radicals). To the best of our knowledge, this is the first study in which coumarin was used as a single chemical probe to detect the formation of both OH radical and other reactive species in a photocatalytic system.

CRediT authorship contribution statement

Abdul Wafi: Investigation, Data curation, Validation, Formal analysis, Writing - original draft. **Erzsébet Szabó-Bárdos:** Conceptualization, Methodology, Writing - original draft, Visualization, Supervision. **Ottó Horváth:** Resources, Writing - review & editing, Funding acquisition, Supervision, Project administration. **Éva Makó:** Investigation, Data curation, Validation, Formal analysis. **Miklós Jakab:** Investigation, Data curation, Validation, Formal analysis. **Balázs Zsirka:** Investigation, Data curation, Validation, Formal analysis.

Declaration of Competing Interest

The authors report no declarations of interest.

Acknowledgment

This work was supported by the Széchenyi 2020 program of the Hungarian Ministry for Innovation and Technology under the GINOP-2.3.2-15-2016-00016 project.

Appendix A. Supplementary data

Supplementary material related to this article can be found, in the online version, at doi:https://doi.org/10.1016/j.jphotochem.2020.112913.

References

[1] S. Guba, V. Somogyi, E. Szabó-Bárdos, Groundwater remediation using biological and photocatalytic methods, Hungarian J. Ind. Chem. 43 (2015) 39–44, https://doi.org/10.1515/hjic-2015-0007.

[2] A.Y.C. Tong, R. Braund, D.S. Warren, B.M. Peake, TiO_2-assisted photodegradation of pharmaceuticals - A review, Cent. Eur. J. Chem. 10 (2012) 989–1027, https://doi.org/10.2478/s11532-012-0049-7.

[3] S. Nagarajan, N.C. Skillen, F. Fina, G. Zhang, C. Randorn, L.A. Lawton, J.T.S. Irvine, P.K.J. Robertson, Comparative assessment of visible light and UV active photocatalysts by hydroxyl radical quantification, J. Photochem. Photobiol. A Chem. 334 (2017) 13–19, https://doi.org/10.1016/j.jphotochem.2016.10.034.

[4] A.L. Linsebigler, G. Lu, J.T. Yates, Photocatalysis on TiO_2 surfaces: Principles, mechanisms, and selected results, Chem. Rev. 95 (1995) 735–758, https://doi.org/10.1021/cr00035a013.

[5] M. Pelaez, N.T. Nolan, S.C. Pillai, M.K. Seery, P. Falaras, A.G. Kontos, P.S. M. Dunlop, J.W.J. Hamilton, J.A. Byrne, K. O'Shea, M.H. Entezari, D.D. Dionysiou, A review on the visible light active titanium dioxide photocatalysts for environmental applications, Appl. Catal. B Environ. 125 (2012) 331–349, https://doi.org/10.1016/j.apcatb.2012.05.036.

[6] J.C. González-Torres, E. Poulain, V. Domínguez-Soria, R. García-Cruz, O. Olvera-Neria, C-, N-, S-, and F-doped anatase TiO_2 (101) with oxygen vacancies: Photocatalysts active in the visible region, Int. J. Photoenergy. 2018 (2018), https://doi.org/10.1155/2018/7506151.

[7] R. Asahi, T. Morikawa, H. Irie, T. Ohwaki, Nitrogen-doped titanium dioxide as visible-light-sensitive photocatalyst: Designs, developments, and prospects, Chem. Rev. 114 (2014) 9824–9852, https://doi.org/10.1021/cr5000738.

[8] J. Marques, T.D. Gomes, M.A. Forte, R.F. Silva, C.J. Tavares, A new route for the synthesis of highly-active N-doped TiO_2 nanoparticles for visible light photocatalysis using urea as nitrogen precursor, Catal. Today. (2019) 36–45, https://doi.org/10.1016/j.cattod.2018.09.002.

[9] L.D. Than, N.S. Luong, V.D. Ngo, N.M. Tien, T.N. Dung, N.M. Nghia, N.T. Loc, V. T. Thu, T.D. Lam, Highly visible light activity of nitrogen doped TiO_2 prepared by sol–gel approach, J. Electron. Mater. 46 (2017) 158–166, https://doi.org/10.1007/s11664-016-4894-6.

[10] Y. Hu, H. Liu, X. Kong, X. Guo, Effect of calcination on the visible light photocatalytic activity of N-doped TiO_2 prepared by the sol-gel method, J. Nanosci. Nanotechnol. 14 (2014) 3532–3537, https://doi.org/10.1166/jnn.2014.8021.

[11] J. Shi, S. Chen, S. Wang, Z. Ye, Sol-gel preparation and visible light photocatalytic activity of nitrogen doped titania, Procedia Eng. (2012) 564–569, https://doi.org/10.1016/j.proeng.2011.12.488.

[12] M.S. Akple, J. Low, Z. Qin, S. Wageh, A.A. Al-Ghamdi, J. Yu, S. Liu, Nitrogen-doped TiO_2 microsheets with enhanced visible light photocatalytic activity for CO_2 reduction, Cuihua Xuebao/Chinese J. Catal. 36 (2015) 2127–2134, https://doi.org/10.1016/S1872-2067(15)60989-5.

[13] T. Suwannaruang, P. Kidkhunthod, N. Chanlek, S. Soontaranon, K. Wantala, High anatase purity of nitrogen-doped TiO_2 nanorice particles for the photocatalytic treatment activity of pharmaceutical wastewater, Appl. Surf. Sci. 478 (2019) 1–14, https://doi.org/10.1016/j.apsusc.2019.01.158.

[14] A. Sanchez-Martinez, O. Ceballos-Sanchez, C. Koop-Santa, E.R. López-Mena, E. Orozco-Guareño, M. García-Guaderrama, N-doped TiO_2 nanoparticles obtained by a facile coprecipitation method at low temperature, Ceram. Int. 44 (2018) 5273–5283, https://doi.org/10.1016/j.ceramint.2017.12.140.

[15] C.S. Kim, J.W. Shin, Y.H. Cho, H.D. Jang, H.S. Byun, T.O. Kim, Synthesis and characterization of Cu/N-doped mesoporous TiO_2 visible light photocatalysts, Appl. Catal. A Gen. 455 (2013) 211–218, https://doi.org/10.1016/j.apcata.2013.01.041.

[16] X. Cheng, X. Yu, Z. Xing, L. Yang, Synthesis and characterization of N-doped TiO_2 and its enhanced visible-light photocatalytic activity, Arab. J. Chem. 9 (2016) S1706–S1711, https://doi.org/10.1016/j.arabjc.2012.04.052.

[17] E. Katoueizadeh, S.M. Zebarjad, K. Janghorban, Synthesis and enhanced visible-light activity of N-doped TiO_2 nano-additives applied over cotton textiles, J. Mater. Res. Technol. 7 (2018) 204–211, https://doi.org/10.1016/j.jmrt.2017.05.011.

[18] O. Sacco, M. Stoller, V. Vaiano, P. Ciambelli, A. Chianese, D. Sannino, Photocatalytic degradation of organic dyes under visible light on n-doped TiO_2 photocatalysts, Int. J. Photoenergy. 2012 (2012), https://doi.org/10.1155/2012/626759.

[19] V. Vaiano, O. Sacco, D. Sannino, P. Ciambelli, Nanostructured N-doped TiO_2 coated on glass spheres for the photocatalytic removal of organic dyes under UV or visible light irradiation, Appl. Catal. B Environ. 170–171 (2015) 153–161, https://doi.org/10.1016/j.apcatb.2015.01.039.

[20] G. Louit, S. Foley, J. Cabillic, H. Coffigny, F. Taran, A. Valleix, J.P. Renault, S. Pin, The reaction of coumarin with the OH radical revisited: Hydroxylation product analysis determined by fluorescence and chromatography, Radiat. Phys. Chem. 72 (2005) 119–124, https://doi.org/10.1016/j.radphyschem.2004.09.007.

[21] H. Czili, A. Horváth, Applicability of coumarin for detecting and measuring hydroxyl radicals generated by photoexcitation of TiO_2 nanoparticles, Appl. Catal. B Environ. 81 (2008) 295–302, https://doi.org/10.1016/j.apcatb.2008.01.001.

[22] G. Žerjav, A. Albreht, I. Vovk, A. Pintar, Revision of terephthalic acid and coumarin as probes for photoluminescent determination of hydroxyl radical formation rate in heterogeneous photocatalysis, Appl. Catal. A Gen. (2020) 117566, https://doi.org/10.1016/j.apcata.2020.117566.

[23] W.J. Chung, D.D. Nguyen, X.T. Bui, S.W. An, J.R. Banu, S.M. Lee, S.S. Kim, D. H. Moon, B.H. Jeon, S.W. Chang, A magnetically separable and recyclable Ag-supported magnetic TiO_2 composite catalyst: Fabrication, characterization, and photocatalytic activity, J. Environ. Manage. 213 (2018) 541–548, https://doi.org/10.1016/j.jenvman.2018.02.064.

[24] H. Klug, L. Alexander, X-ray diffraction procedures: For polycrystalline and amorphous materials, 2nd Edition, Wiley-VCH, New York, USA, 1974, p. 992, http://scholar.google.com/scholar?hl=en&btnG=Search&q=intitle:X-ray+diffraction+procedures#2.

[25] F.X. Nobre, W.A. Gil Pessoa, Y.L. Ruiz, V.L. Imbiriba Bentes, M.O. Silva-Moraes, T. M. Costa Silva, M.L. Miranda Rocco, D.R. González Larrudé, J.M.E. de Matos, P. R. da Costa Couceiro, W.R. Brito, Facile synthesis of nTiO_2 phase mixture: Characterization and catalytic performance, Mater. Res. Bull. 109 (2019) 60–71, https://doi.org/10.1016/j.materresbull.2018.09.019.

[26] Y.Y. Gurkan, N. Turkten, A. Hatipoglu, Z. Cinar, Photocatalytic degradation of cefazolin over N-doped TiO_2 under UV and sunlight irradiation: Prediction of the reaction paths via conceptual DFT, Chem. Eng. J. 184 (2012) 113–124, https://doi.org/10.1016/j.cej.2012.01.011.

[27] E. Pérez, M.F. Torres, G. Morales, V. Murgia, E. Sham, Synthesis of N-TiO_2 effect of the concentration of nitrogen in the band gap, Procedia Mater. Sci. (2015), https://doi.org/10.1016/j.mspro.2015.04.121.

[28] G. Wang, L. Xu, J. Zhang, T. Yin, D. Han, Enhanced photocatalytic activity of TiO_2 powders (P25) via calcination treatment, Int. J. Photoenergy. 2012 (2012), https://doi.org/10.1155/2012/265760.

[29] J. Yu, G. Wang, Hydrothermal synthesis and photocatalytic activity of mesoporous titania hollow microspheres, J. Phys. Chem. Solids. 69 (2008) 1147–1151, https://doi.org/10.1016/j.jpcs.2007.09.024.

[30] N.A. Sabri, M.A. Nawi, W.I. Nawawi, Porous immobilized C coated N doped TiO_2 containing in-situ generated polyenes for enhanced visible light photocatalytic activity, Opt. Mater. (Amst). 48 (2015) 258–266, https://doi.org/10.1016/j.optmat.2015.08.010.

[31] G. Liu, X. Wang, L. Wang, Z. Chen, F. Li, G.Q. Max Lu, H.M. Cheng, Drastically enhanced photocatalytic activity in nitrogen doped mesoporous TiO_2 with abundant surface states, J. Colloid Interface Sci. 334 (2009) 171–175, https://doi.org/10.1016/j.jcis.2009.02.047.

[32] X.F. Lei, X.X. Xue, H. Yang, C. Chen, X. Li, M.C. Niu, X.Y. Gao, Y.T. Yang, Effect of calcination temperature on the structure and visible-light photocatalytic activities of (N, S and C) co-doped TiO_2 nano-materials, Appl. Surf. Sci. 332 (2015) 172–180, https://doi.org/10.1016/j.apsusc.2015.01.110.

[33] H. Wu, J. Ma, C. Zhang, H. He, Effect of TiO_2 calcination temperature on the photocatalytic oxidation of gaseous NH 3, J. Environ. Sci. (China). 26 (2014) 673–682, https://doi.org/10.1016/S1001-0742(13)60441-6.

[34] T. Ohno, K. Sarukawa, K. Tokieda, M. Matsumura, Morphology of a TiO_2 photocatalyst (Degussa, P-25) consisting of anatase and rutile crystalline phases, J. Catal. 203 (2001) 82–86, https://doi.org/10.1006/jcat.2001.3316.

[35] W. Junwei, Z. Wei, Z. Yinqing, L. Shuangxi, An efficient two-step technique for nitrogen-doped titanium dioxide synthesizing: Visible-light-induced photodecomposition of methylene blue, J. Phys. Chem. C. 111 (2007) 1010–1014, https://doi.org/10.1021/jp066156o.

[36] T. Suwannaruang, K. Kamonsuangkasem, P. Kidkhunthod, P. Chirawatkul, C. Saiyasombat, N. Chanlek, K. Wantala, Influence of nitrogen content levels on structural properties and photocatalytic activities of nanorice-like N-doped TiO_2 with various calcination temperatures, Mater. Res. Bull. 105 (2018) 265–276, https://doi.org/10.1016/j.materresbull.2018.05.010.

[37] G. Yang, Z. Jiang, H. Shi, T. Xiao, Z. Yan, Preparation of highly visible-light active N-doped TiO_2 photocatalyst, J. Mater. Chem. 20 (2010) 5301–5309, https://doi.org/10.1039/c0jm00376j.

[38] J. Zhang, Y. Nosaka, Mechanism of the OH radical generation in photocatalysis with TiO_2 of different crystalline types, J. Phys. Chem. C. 118 (2014) 10824–10832, https://doi.org/10.1021/jp501214m.

[39] C.Y. Wu, K.J. Tu, J.P. Deng, Y.S. Lo, C.H. Wu, Markedly enhanced surface hydroxyl groups of TiO_2 nanoparticles with Superior water-dispersibility for photocatalysis, Materials (Basel). 10 (2017), https://doi.org/10.3390/ma10050566.

[40] R.L. Narayana, M. Matheswaran, A.A. Aziz, P. Saravanan, Photocatalytic decolourization of basic green dye by pure and Fe, Co doped TiO_2 under daylight illumination, Desalination. 269 (2011) 249–253, https://doi.org/10.1016/j.desal.2010.11.007.

[41] J. Yu, L. Zhang, B. Cheng, Y. Su, Hydrothermal preparation and photocatalytic activity of hierarchically sponge-like macro-/mesoporous Titania, J. Phys. Chem. C. 111 (2007) 10582–10589, https://doi.org/10.1021/jp0707889.

[42] M.R.D. Khaki, M.S. Shafeeyan, A.A.A. Raman, W.M.A.W. Daud, Application of doped photocatalysts for organic pollutant degradation - A review, J. Environ. Manage. 198 (2017) 78–94, https://doi.org/10.1016/j.jenvman.2017.04.099.

[43] J.H. Shen, J.J. Horng, Y.S. Wang, Y.R. Zeng, The use of reactive index of hydroxyl radicals to investigate the degradation of acid orange 7 by Fenton process, Chemosphere. 182 (2017) 364–372, https://doi.org/10.1016/j.chemosphere.2017.05.043.

[44] B.C.C. Rutely, J.M. Fontmorin, Z. Tang Walter, D.B. Xochitl, S. Mika, C. Burgos Castillo Rutely, J.M. Fontmorin, Z. Tang Walter, D.B. Xochitl, S. Mika, Towards reliable quantification of hydroxyl radicals in the Fenton reaction using chemical probes, RSC Adv. 8 (2018) 5321–5330, https://doi.org/10.1039/c7ra13209c.

[45] K. ichi Ishibashi, A. Fujishima, T. Watanabe, K. Hashimoto, Quantum yields of active oxidative species formed on TiO_2 photocatalyst, J. Photochem. Photobiol. A Chem. 134 (2000) 139–142, https://doi.org/10.1016/S1010-6030(00)00264-1.

[46] E.J. Land, T.G. Truscott, Triplet excited state of coumarin and 4'5' dihydropsoralen : Reaction with nucleic acid bases and amino acids, Photochem. Photobiol. 29 (1979) 861–866, https://doi.org/10.1111/j.1751-1097.1979.tb07783.x.

[47] G.V. Buxton, C.L. Greenstock, W.P. Helman, A.B. Ross, Critical Review of rate constants for reactions of hydrated electrons, hydrogen atoms and hydroxyl

radicals ($^{\cdot}OH/^{\cdot}O^{-}$) in aqueous solution, J. Phys. Chem. Ref. Data. 17 (1988) 513–886, https://doi.org/10.1063/1.555805.

[48] E. Szabó-Bárdos, H. Czili, A. Horváth, Photocatalytic oxidation of oxalic acid enhanced by silver deposition on a TiO_2 surface, J. Photochem. Photobiol. A Chem. 154 (2003) 195–201, https://doi.org/10.1016/S1010-6030(02)00330-1.

[49] J. Rabani, S.O. Nielsen, Absorption spectrum and decay kinetics of O_2- and HO_2 in aqueous solutions by pulse radiolysis, J. Phys. Chem. 73 (1969) 3736–3744, https://doi.org/10.1021/j100845a030.

[50] A.A. Frimer, G. Aljadeff, P. Gilinsky-Sharon, Reaction of Coumarins with Superoxide Anion Radical ($^{\cdot}O_2^{-}$): Facile entry to o-coumarinic acid systems, Isr. J. Chem. 27 (1986) 39–44, https://doi.org/10.1002/ijch.198600007.